

Effects of Phospholipid Composition on the Transfer of a Small Cationic Peptide Across a Model Biological Membrane

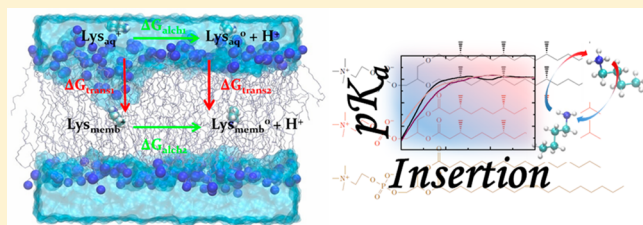
Daniel Bonhenry,^{†,‡} Mounir Tarek,^{*,†,‡} and François Dehez^{*,†,‡}

[†]Université de Lorraine, SRSMC, UMR 7565, Vandoeuvre-lès-Nancy, F-54500, France

[‡]CNRS, SRSMC, UMR 7565, Vandoeuvre-lès-Nancy, F-54500, France

Supporting Information

ABSTRACT: The transfer of a lysine amino acid analogue across phospholipid membrane models was investigated using molecular-dynamics simulations. The evolution of the protonation state of this small peptide as a function of its position inside the membrane was studied by determining the local pK_a by means of free-energy calculations. Permeability and mean-first-passage time were evaluated and showed that the transfer occurs on the submillisecond time scale. Comparative studies were conducted to evaluate changes in the pK_a arising from differences in the phospholipid chemical structure. We compared, hence, the effect of an ether vs an ester linkage of the lipid headgroup as well as linear vs branched lipid tails. The study reveals that protonated lysine residues can be buried further inside an ether lipid membrane than an ester lipid membrane, while branched lipids are found to stabilize less the charged form compared to their unbranched lipid chain counterparts.



INTRODUCTION

The membrane constitutes an important part of the cell. Not only does it give support for trans-membrane proteins to anchor in but it acts also as a natural barrier against molecules and prevents them from going in or out of the cell. Such is the case for many ions, charged compounds, and large polar molecules, e.g., drugs that in order to be effective, need to cross this barrier. Different strategies have been developed during the past decades to transfer molecules of variable sizes and chemical properties across membranes of a cell or of unilamellar vesicles.

For instance, one strategy is to anchor an active compound on a platform, such as carbon nanotubes or fullerenes.^{1–4} These compounds are known to be highly hydrophobic and thus can facilitate the insertion of a given bound hydrophilic drug inside the membrane. Optimizing the balance between hydrophobic and hydrophilic properties of a given molecular construct is crucial to enhancing its propensity to cross membranes and to reach its target located in the cell. Within the same goal of delivering drugs or small fragments of DNA inside a cell, cell-penetrating peptides (CPPs) have been recently the object of active research. They are short polycationic peptides (lysine or arginine rich) of 10 to 50 amino acids which are capable of crossing the cellular plasma membrane.^{5–7} Like carbon-based nanostructures, they can be used as a plate-form to anchor drugs or other sensors to facilitate their passage across biological membranes. Still, if carbon-based vectors or CPP appear to be good candidates to enhance the transfer of any drug inside a cell, their use is limited by their cell specificity, stability, immunogenicity, and toxicity.^{8–11}

Another strategy consists of loading the drug inside a liposome. It has been observed that during the passive loading

of a liposome, rapid permeation of noncharged drugs across its barrier (membrane) may occur. The active loading is achieved by increasing the pH in the outer environment of the liposome in order to deprotonate the charge substrate, facilitating the drug permeation inside the liposome where pH conditions favor the substrate protonated state that remains trapped. It has been shown for instance that for a pH gradient no higher than 3 units, the concentration of a weak base can be maintained 1000 fold higher inside a vesicle than outside.¹²

Regardless of the method used to vectorize small fragments or molecules inside cell compartments, understanding the interaction of basic amino acid residues with biological membranes and their behavior once they penetrate the hydrophobic core is of crucial importance. We focus here on titratable residues, i.e., amino acids that can exist in two different states depending on the environment. They may lose or gain a proton, leading to a deprotonated form or to a protonated form, the latter carrying a net charge. One of such residues, arginine, was subject to extensive studies because of its ubiquitous presence in the S4 helix of voltage gated ion channels. Interesting setups have been proposed to evaluate the cost to insert such a residue inside a membrane^{13–15} in order to understand how this amino acid, apparently protonated, can be exposed to the hydrophobic core of the membrane. Molecular-dynamics simulations and free-energy calculations demonstrated that arginine remains protonated even at the center of the bilayer. Such a difference is rooted in (*i*) the larger pK_a of arginine ($pK_a = 12.48$) with respect to lysine ($pK_a = 10.54$) and

Received: July 3, 2013

Published: November 8, 2013

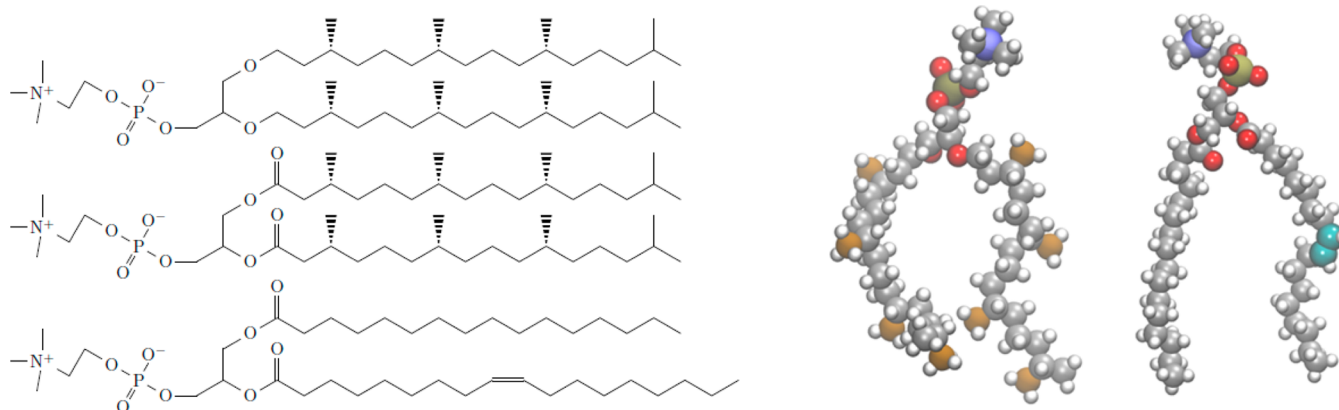


Figure 1. Left: Representation of the lipid used. From top to bottom: ether-DPhPC, DPhPC, and POPC (see density profiles of the corresponding bilayers SM.1). Right: DPhPC-ether molecule and POPC molecule (from right to left). Carbon, gray; oxygen, red; nitrogen, blue; phosphorus, brown; methyl group of DPhPC, ochre; double bond, cyan. Rendering done with VMD.³⁸

(ii) the largest free energy barrier encountered by the unpronated form of arginine compared to the unprotonated lysine.¹⁶ This feature has been recently assessed by experiments using a transmembrane α -helix and site-directed mutagenesis.¹⁷ The possibility that an assisted transfer by another transmembrane protein enabling arginine to tunnel the high energy barrier was considered.¹⁸

We have chosen here to concentrate on the lysine amino acid analogue that along arginine is another basic compound, which was suggested to deprotonate inside a membrane.¹⁶ This lysine analogue can be regarded as an independent part of much more complex constructs since this amino acid is often found in a variety of drug vectors or CPP.^{19,20} The aim of this work is to study the influence of the various environments offered by a biological membrane and determine how they can modulate the lysine protonation state independently from the rest of a much more complex drug that can be possibly attached to it. Considering that biological membranes are impermeable to ions and charged compounds but can let a lipophilic neutral molecule go inside the bilayer hydrophobic core, switching from the charged to the neutral state of a given titratable molecule is possibly underlying the overall translocation process. The transfer of small peptides such as amino acid analogues is an old topic of interest. Even if substantial progress has been made rationalizing the partitioning and the transfer of molecules across a hydrophobic/water interface, phenomena linked to drug vectorization remain unclear. A few years back, various groups estimated the cost of inserting amino acids analogues inside phospholipid membranes using extensive molecular-dynamics simulations and free-energy calculations. Studies concerned not only the effect of the membrane lipid composition by considering different kinds of lipid headgroups and tails with an increasing number of unsaturations^{21,22} but also the effect of additives such as cholesterol on the permeability and the transfer of organic compounds.²³

For instance, an increase in the concentration of cholesterol was shown to lead to an increase of the pK_a of an arginine analogue inside the membrane.²⁴ Membrane permeability is known to decrease as the concentration in cholesterol increases. Cholesterol also increases the ordering and the packing of the lipids, thus leading to a decrease in the area per lipid and an increase of the stiffness. It has also been pointed out that cholesterol can modify the total dipole potential of the membrane.²⁵

Which of these effects leads to the increase of pK_a remains unclear though. We propose here to extend these investigations by studying the transfer of a lysine analogue in a membrane composed of archaea lipid. These molecules are mainly present in a category of living organism known as archaea bacteria, which constitutes one of the three main domains of the living world with eukaryotes and bacteria.^{26,27} From a chemical perspective, archaea lipids bear an ether function in lieu of an ester linkage between headgroups and tails. This relatively small difference has an important impact on the properties of the membrane,^{28,29} the overall membrane dipole potential for ether-DPhPC [ether-linked diphyanoyl-phosphatidyl-choline (PC)] is 2-fold lower than for DPhPC (ester-linked-diphyanoyl-PC).^{30,31} Furthermore, the tail of archaea lipids differs from those of usual lipids in that instead of having methylene groups along the acyl chains, they carry methyl functions which refer them to branched lipids. As a result, the stiffness of membranes composed of such lipids increases and gives archaea bacteria a much greater stability at high ionic concentrations and/or other extreme conditions.^{32,33} On the other hand, the presence of branched chains increases the stability and decreases the permeability³⁴ of the bilayers which is related to the slower conformational motion of the lipid tails. It has been demonstrated by experiments that translocation of water,³⁵ ions,³⁶ and dyes³⁷ is noticeably decreased in a bilayer composed of branched chains compared to linear lipids.

Here, we studied the evolution of the protonation state of an amino acid analogue (amino acid truncated at the beta carbon) inside archaea model membranes. This simple amino, building block of many engineered molecular vectors, is employed as a paradigmatic system to decipher the role of protonation in the transfer of cell-penetrating peptides and vectorized drugs into biological cells.

METHODS

Three different types of lipids were used to construct model membranes: DPhPC with either ester or ether linkage (ester/ether-DPhPC) was used to investigate the influence of the membrane dipole potential, while palmitoyl oleyl-phosphatidyl choline (POPC) lipid was considered to compare the effects of lipid tails (see Figure 1).

In order to be consistent with previous solvation studies^{16,39,40} of amino acids, patches of 64 fully hydrated lipid bilayers were used for each system. For each model

membrane, free energies of transfer of the charged and the neutral forms of lysine analogue between bulk and the interior of the membrane were systematically determined. The evaluation of the pK_a as a function of the depth insertion inside the membrane was inferred from these calculations. The CHARMM27⁴¹ force field was used for the peptide, while CHARMM36⁴² served to describe lipids; the TIP3P model was employed for the water. The parameters derived by Shinoda et al.³⁰ for DPhPC (with ether linkage) were adopted. All the simulations were conducted at constant pressure (1 atm) and constant temperature (300 K) employing the Langevin piston method^{43,44} and the Langevin dynamics. No surface tension was applied since the CHARMM36 version for lipids reproduces correct area per lipid in the NPT ensemble³⁸ and no corrections for the dihedral angles are present (no CMAP). Long-range electrostatic interactions were calculated using the particle mesh Ewald method.^{45,46} The long-range and short-range forces were calculated respectively every 4 and 2 fs using the RESPA integrators.⁴⁷ Covalent hydrogen bonds were restrained by using the SHAKE⁴⁸ algorithm. All trajectories were generated with NAMD.⁴⁹ Setups were built by using the packmol software.⁵⁰ Heating for half a nanosecond at 380 K followed by slowly cooling to the desired temperature using different temperature steps of 2 ns (360 K, 320 K, and finally 300 K, the desired temperature) were performed. Equilibration for 25 ns was done after a plateau was reached by the area per lipid at the expected experimental value.

pK_a Calculations. Considering the following chemical equilibrium



where the reaction features the protonated lysine LysH^+ , its neutral conjugated basis Lys^0 , and the proton H^+ resulting from the deprotonation. K_a , the equilibrium constant related to this acid–base reaction, can be expressed as

$$K_a = \frac{[\text{Lys}^0][\text{H}^+]}{[\text{LysH}^+]} \quad (2)$$

where [...] are the concentrations relative to the product and the reactants. The pK_a associated with this reaction can be expressed as¹⁵

$$\begin{aligned} pK_a &= -\log K_a = -\log \frac{[\text{Lys}^0][\text{H}^+]}{[\text{LysH}^+]} \\ &= \frac{(G_{\text{Lys}}^0 + G_{\text{H}^+}) - G_{\text{LysH}^+}}{2.303 \times RT} \\ &= \frac{\Delta G_{\text{bulk}}}{2.303 \times RT} \end{aligned} \quad (3)$$

where $G_{\text{Lys}}^0(z)$, $G_{\text{LysH}}(z)$, and G_{H^+} are the free energies related respectively to the lysine analogue in its neutral and protonated forms and to the proton, ΔG_{bulk} is the free energy difference associated with the deprotonation reaction in bulk water, R is the perfect gas constant, and T is the temperature. Considering the transfer of the lysine across a lipid bilayer, its pK_a depends on the local environment and can be expressed as a function of its insertion depth within the membrane z . Evaluating the contribution for the proton is not straightforward; thus rather than estimating a pK_a at position z , a pK_a shift (ΔpK_a) can be evaluated and added to a reference pK_a value of the lysine in bulk water.

By decomposing the free-energy difference ΔG associated with reaction 1 at a position z ,

$$\begin{aligned} \Delta G(z) &= (G_{\text{Lys}}^0(z) + G_{\text{H}^+}) - G_{\text{LysH}^+}(z) \\ &= (G_{\text{Lys}}^0(z) + G_{\text{H}^+}) - G_{\text{LysH}^+}(z) \\ &\quad + (G_{\text{Lys}}^0_{\text{bulk}} + G_{\text{H}^+}) - G_{\text{LysH}^+_{\text{bulk}}} \\ &\quad - (G_{\text{Lys}}^0_{\text{bulk}} + G_{\text{H}^+}) + G_{\text{LysH}^+_{\text{bulk}}} \end{aligned} \quad (4)$$

Here, the free energy associated with the reaction in bulk water is explicitly expressed, and it is assumed that the free energy associated with the deprotonation does not depend on the insertion depth and implies that the proton will always end up in bulk water. The difference in the free energy between the protonated state and the neutral state thus only depends on the difference between the free energy to solvate the lysine analogue in bulk water and inside the membrane.⁵¹ The pK_a at a position z can thus be written as

$$\begin{aligned} pK_a(z) &= \frac{1}{2.303 \times RT} \Delta G(z) \\ &= \frac{1}{2.303 \times RT} [(G_{\text{Lys}}^0_{\text{bulk}} + G_{\text{H}^+}) - G_{\text{LysH}^+_{\text{bulk}}} \\ &\quad + (G_{\text{Lys}}^0(z) - G_{\text{Lys}}^0_{\text{bulk}}) \\ &\quad - (G_{\text{LysH}^+}(z) - G_{\text{LysH}^+_{\text{bulk}}})] \\ &= \frac{1}{2.303 \times RT} [\Delta G_{\text{bulk}} + \Delta \Delta G(z)] \\ &= pK_{a_{\text{bulk}}} + \Delta pK_a(z) \end{aligned} \quad (5)$$

where $\Delta \Delta G(z)$ represents the free-energy difference between a deprotonation occurring in the bulk and at a position z in the membrane, $pK_{a_{\text{bulk}}}$ is the experimental pK_a value in water (10.77),⁵² and ΔpK_a is the shift reflecting the change of environment with respect to the bulk situation. Thus, determining the pK_a amounts to the determination of the solvation free energy of the lysine amino acid analogue in its two different states. In order to calculate ΔpK_a , we resort to a thermodynamic cycle (Figure 2), following which, there are two roads toward the estimation of the overall free energy difference,

$$\begin{aligned} \Delta \Delta G(z) &= \Delta G_{\text{alch1}} - \Delta G_{\text{alch2}}(z) \\ &= \Delta G_{\text{trans1}}(z) - \Delta G_{\text{trans2}}(z) \end{aligned} \quad (6)$$

Here, ΔG_{alch1} and $\Delta G_{\text{alch2}}(z)$ are the free-energy differences associated with the deprotonation reaction estimated in the bulk water and at an insertion depth z in the membrane, respectively. $\Delta G_{\text{trans1}}(z)$ and $\Delta G_{\text{trans2}}(z)$ are the free-energy differences associated with the translocation across the membrane of the neutral and the protonated lysine amino acid analogue, respectively.

$\Delta pK_a(z)$ may be estimated directly as a function of ΔG_{alch1} and $\Delta G_{\text{alch2}}(z)$ corresponding to the horizontal arrows of the cycle (Figure 2). The alchemical transformation is a robust method and has already shown its reliability in simulations close to our case.¹⁸ Still, determining the variation of the lysine pK_a as a function of the environment remains computationally fastidious as it requires the full alchemical transformation to be carried out at many positions along the normal to the bilayer. Here, ΔG_{alch2} will be estimated only for a limited set of depth

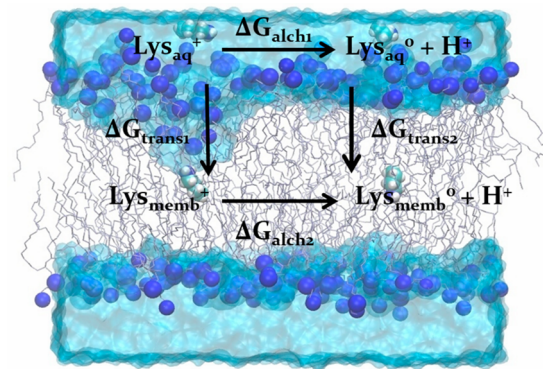


Figure 2. Thermodynamic cycle used to estimate the pK_a of a lysine analogue at a given depth inside a membrane. The horizontal paths correspond to the alchemical transformation of a charged lysine to its neutral form. The vertical paths correspond to the diffusion of either the charged or the neutral species along the normal to the bilayer. The proton is not explicitly taken into account during the simulation; the pK_a inside the membrane is inferred by computing a shift, reflecting the contribution of the environments.

insertions and will be mainly employed to control the validity of ΔpK_a estimated following the geometrical path (vertical transformation in Figure 2). The variation of ΔpK_a as a function of the insertion depth can be inferred from the difference between two potentials of mean force associated with the translocation of the charged and the neutral substrates, respectively.

Free Energy Calculations. Free energy calculations were conducted using either the free energy perturbation^{53,54} (FEP) formalism or the ABF method as implemented in NAMD.^{55–58} Alchemical transformation consists of mutating the potential energy function of a molecule A into the potential of another molecule B by slowly switching a thermodynamic coupling parameter, λ , from 0 to 1. The free-energy associated with this mutation can be calculated by using the perturbation formalism

$$\Delta G_{A \rightarrow B} = -\frac{1}{\beta} \exp\{-\beta[H_A(x, p_x) - H_B(x, p_x)]\}_A \quad (7)$$

where H_A and H_B are the Hamiltonians describing A and B , respectively, $\beta = 1/k_B T$, and the brackets $\langle \dots \rangle_A$ denote an average over the state A .

Alchemical transformations were conducted at different positions of the lysine analogue inside the bilayer. For each localization (L0–LS, water—see Table 1), the amino acid was restrained to a slab 2 Å wide around its position by imposing barriers along the reaction coordinate as implemented in the colvars module of NAMD. The transformations were performed in 40 even consecutive windows ($\delta\lambda$). Depending on the position of the peptide inside the membrane, longer sampling was needed for windows close to the center of the

bilayer, since major perturbations of the membrane occur when the charged compound is far from the headgroup region.¹⁶ Hence, ~2 ns was sufficient for the calculations to converge close to the bulk water region, and up to 100 ns calculations were conducted for transformations 10 Å beneath the carbonyl groups.

A soft-core potential⁵⁹ was used to avoid any end point catastrophes. For the set up protocols adopted, the total charge of the system varies between the start and end of the calculations, and as highlighted by previous studies, special care has to be taken. Indeed, due to the artificial periodicity of the system, the free-energy differences evaluated can be contaminated by the contribution of the charge images. An analytical formula was derived in the case of the cubic simulation box, which led to a size dependent box correction $\xi_{\text{Ewald}} = -2.837/L$, where L is the length of the box. This error was evaluated to be around or less than 0.5 kcal mol⁻¹ for systems close to our size.^{18,24}

In the ABF^{57,58,60} method, the mean force acting along a reaction coordinate ξ is evaluated during the simulation.

$$\frac{dA(\xi)}{d\xi} = \left\langle \frac{\partial V(x)}{\partial \xi} - \frac{1}{\beta} \frac{\partial \ln|J|}{\partial \xi} \right\rangle_\xi = -\langle F_\xi \rangle_\xi \quad (8)$$

where $V(x)$ is the potential energy function and J the Jacobian used for the transformation from the Cartesian coordinates to the generalized coordinates. The chosen reaction coordinate is discretized in small bins $\delta\xi$ in which the force F_ξ is estimated. The opposite of this force is then applied to the system, thus allowing in theory for a uniform sampling all along the reaction coordinate. The sampling along ξ is driven by the self-diffusion of the system, assuming that no orthogonal slow degrees of freedom are hidden and thus can disrupt the uniform sampling. Since the biasing force is linked to the free-energy derivative, the integration of the force leads to the free-energy variation along the chosen reaction coordinate.

Here, the reaction coordinate is the projection on the normal of the bilayer of the distance between the center of mass of the lysine and the center of mass of the membrane. It was split into three nonoverlapping windows spanning from 0 to 33 Å; two of them (10 Å each) were located inside the membrane corresponding to the tails and the headgroup region, and the last window encompassing the outermost part of the headgroup region and bulk water was 13 Å wide. Free-energy calculations performed on similar systems emphasized the need of extensive sampling to obtain converged potentials of mean force (PMF).⁶¹ A total of 20 to 30 ns MDs were sufficient to obtain converged estimates of the free energies in the water/headgroup region, and up to 100 ns simulations were performed inside the membrane because of slow convergence induced by the slow membrane reorganization. A total of ~0.5 μs of sampling was required for each free-energy profile.

Table 1. Free Energy Difference between the Charged Form and the Neutral Form of the Lysine Amino Acid Analogue from Alchemical Transformations at Different Positions (with Respect to the Center of the Bilayer) along the Axis Perpendicular to the Membrane

index	L0	L1	L2	L3	L4	L5	bulk water
depth (Å)	1.8 ± 0.4	4.6 ± 0.5	9.5 ± 0.5	15.8 ± 0.7	20.2 ± 1.3	25.3 ± 1.2	32.1 ± 1.2
ΔG (kcal mol ⁻¹)	39.7^a	44.16^a	47.79 ± 0.11^b	48.78 ± 0.08^b	48.77 ± 0.09^b	48.26 ± 0.06^b	48.71 ± 0.05^b

^aOnly mutations from charged molecule to neutral molecule. ^bForward and backward transformations, uncertainty evaluated using the BAR estimator in the ParseFEP⁶⁷ plugin in VMD.

Kinetics. Free energy is a thermodynamic quantity that determines the energetic cost of a process, e.g., a chemical change or diffusion along a predetermined path. Kinetics on the other hand describe how fast this process occurs. Two quantities have been considered to fully describe the translocation of the lysine amino acid analogue across a membrane. The permeability P , which corresponds to the speed at which a compound would cross the lipid membrane, and the rate constant, associated with this transfer. For small molecules or organic compounds, the solubility-diffusion model was shown to be appropriate to describe their kinetics of transfer across a bilayer.^{62–64}

According to this model, the transfer of a compound across a membrane occurs in three different steps. First, the molecule coming from the bulk reaches and binds to the membrane interface. Then it dissolves inside the hydrophobic core of the membrane and binds to the other side of the bilayer. Finally, the molecule leaves the interface and diffuses out to the opposite bulk region. Specifically, according to this model, diffusion through the membrane occurs by jumps between available pockets (free volume); the permeability P is then expressed as

$$P = 1 / \int_{z_1}^{z_2} \frac{\exp(\Delta G(z)/k_B T)}{D_z(z)} dz \quad (9)$$

where R is the resistance of the membrane to the permeation defined as the invert of the permeation, ΔG is the free energy difference, k_B is the Boltzmann constant, T is the temperature, and $D_z(z)$ is the diffusion coefficient at a distance z . We used here a method recently developed by Hummer⁶⁵ in which the autocorrelation position function of a harmonically restrained amino acid is used to determine the coefficient diffusion at a certain position using the following equation:

$$D(\xi_i) = \frac{\langle \delta\xi^2 \rangle_i}{\tau_i} \quad (10)$$

where τ_i is the correlation time of the reaction coordinate ξ at the position i , defined as

$$\tau_i = \frac{\int_0^\infty \langle \delta\xi(t) \delta\xi(0) \rangle_i dt}{\langle \delta\xi^2 \rangle_i} \quad (11)$$

This is valid in the case of an overdamped harmonic oscillator. To obtain a diffusion profile across the membrane, the lysine amino acid analogue was restrained successively every Ångström along the normal to the bilayer with a restraint potential of 10 kcal mol⁻¹ Å², and the autocorrelation function was analyzed over a 4 ns run.

Rate constants, which quantify the fraction of molecules that cross the bilayer per unit time, were computed using the formalism of Wang et al.⁶⁶ In this model, a discrete form of the Fokker–Planck equation is used where the reaction coordinate is split into a finite number n of sites with a probability p_n to find the system at site n . These probabilities obey the equation:

$$\frac{dp_n}{dt} = - (B_{n-1/2} + F_{n+1/2})p_n + F_{n-1/2}p_{n-1} + B_{n+1/2}p_{n+1} \quad (12)$$

where F_n and B_n are respectively the forward and the backward transition rates between two sites. The transition can hence be evaluated according to

$$F_n = \frac{D_n}{\Delta x^2} \frac{-\alpha}{\exp(-\alpha) - 1} \quad (13)$$

$$B_n = \frac{D_n}{\Delta x^2} \frac{\alpha}{\exp(\alpha) - 1} \quad (14)$$

where $\alpha = -\Delta G/k_B T$, Δx is the size of the bin, and D_n is the diffusion coefficient.

RESULTS

Transfer Across a POPC Lipid Bilayer. As previously reported by several authors, a specific phenomenon associated with the transfer of a net charge inside a membrane was observed during the transfer of the lysine-charged analogue: water defects and phosphorus headgroups are pulled inside the membrane, allowing for the charged moiety to remain solvated (Figure 4). Indeed, the amino acid analogue possesses a relatively long carbonated chain, which allows the charged amine function to snorkel in the direction of the bulk water; i.e., when the charged lysine amino acid is dragged inside the membrane, the amine function remains directed toward the interface while the carbons point toward the center of the membrane. In contrast, in the case of the neutral form, minor water defects occur; they do not span all the membrane but stay localized to 2–3 Å beneath the lipid carbonyl region.

As expected, the free energy required to transfer the charged amino acid analogue inside a membrane is higher than the neutral one (Figure 3). The PMF associated with the neutral

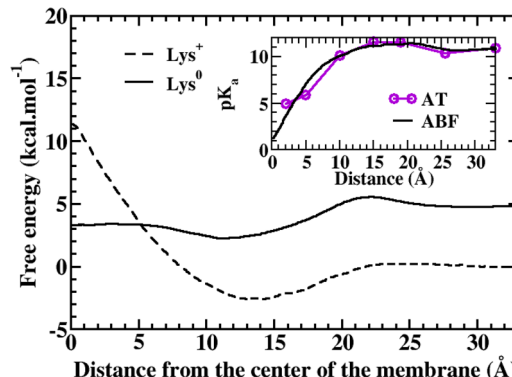


Figure 3. Adaptive Biasing Force (ABF) free energy profiles for a charged lysine analogue (dashed black curve) and a neutral lysine analogue (solid black curve) as a function of the distance between the center of mass of a POPC membrane and the center of mass of the peptide. The neutral profile was shifted by the free-energy difference associated with the deprotonation reaction in the bulk. Inset: pK_a profile for the lysine as a function of the depth insertion in the membrane obtained with the ABF method (dark solid curve) and Alchemical Transformation (AT; purple solid curve and circles). Each circle represents a transformation region (see Table 1).

form is in agreement with other profiles obtained with different methods and force fields.^{16,40} It shows a small barrier at the interface (~0.5 kcal mol⁻¹) arising from the ordering of the headgroup region, followed by a well of ~3 kcal mol⁻¹, and a plateau corresponding to the lipids tails region. The PMF corresponding to the charged compound exhibits a small well at 10 Å and then a high free-energy barrier of 15 kcal mol⁻¹. This huge barrier occurring at the center of the bilayer is consistent with other observations for charged compounds transferred from bulk water to a hydrophobic medium.^{22,68}

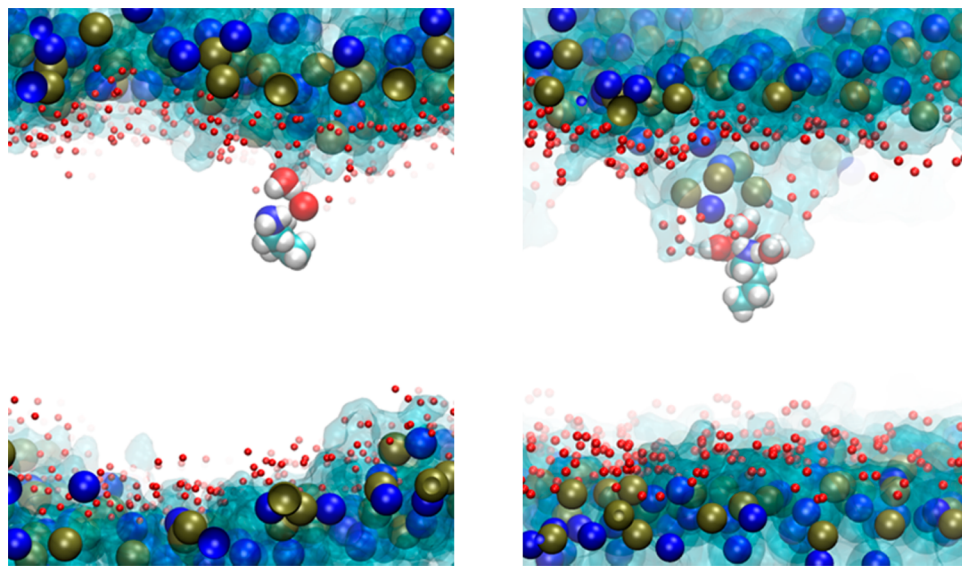


Figure 4. Perturbations induced on the membrane due to the transfer of the lysine in its two protonated states across the membrane. Snapshots from simulations: (left) water molecules hydrogen bonding with the neutral lysine beneath the interface and (right) water finger let the charged lysine be solvated while phosphorus head groups are pulled inside the hydrophobic part of the membrane. VMD³⁸ software was used for the rendering. Brown sphere, phosphate; blue sphere, nitrogen.

The pK_a profiles obtained using the ABF method and those extracted from the alchemical transformation procedure (cf Table 1) are reported in Figure 3 and essentially agree except near the center of the bilayer. This discrepancy stems mainly from difficulties to sample correctly the phase space during the alchemical transformation due to the slow reorganization of the lipids and perturbations induced during the insertion of the peptides across the interface as depicted in Figure 4.

Noticeably, both methods give similar results in the region where the pK_a value is ~ 7 . A drop of the pK_a occurs when the lysine penetrates the hydrophobic core of the membrane. Thus, the proportion of neutral lysine becomes more and more important as the center of the bilayer is reached. In fact, the position where the populations of the neutral and the protonated forms equal each other lies around 6 Å from the bilayer center. At this location, the pK_a equals the pH, and therefore, according to the Henderson–Hasselbach equation, $[Lys^+] = [Lys^0]$. Li et al. recently computed PMF translocation for both the neutral and lysine analogues; their results nicely match our PMFs obtained with ABF.⁶⁹

Transfer Rates through the Bilayer. To evaluate more completely the translocation process of the lysine, the permeability and rate constants of the amino acid analogue across POPC bilayers were determined. The diffusion profiles (SM.2), plotted as a function of the position of the lysine analogue, do not depend on the protonation state. When the lysine analogue enters the membrane, its diffusion coefficient drops down compared to its value in solution, a process already observed for various organic compounds in different membranes.⁷⁰ Combining diffusion and free-energy profiles allows for estimating the kinetics of the diffusion process.

The neutral lysine analogue permeates the lipid membrane faster than its protonated form at a permeation rate of 42.96 cm s⁻¹ and 6.8×10^{-9} cm s⁻¹, respectively. The permeation coefficient of a charged lysine side-chain across DMPC (dimyristoylphosphatidylcholine) large unilamellar vesicles (LUVs) was estimated⁷⁰ to be 3.7×10^{-11} cm s⁻¹ at pH = 7. Permeation for other unaltered amino acids was found to be in

the same range,⁷¹ owing to the high energy cost to bring a charge inside the hydrophobic core of the membrane. Other permeability coefficients for small organic compounds were estimated both experimentally and using simulations.^{62,72,73} Depending on the molecule and the simulation conditions or the experimental protocol, the permeabilities range from 10 cm s⁻¹ to 10^{-4} cm s⁻¹, with discrepancies between simulations and experiments reaching as much as 10^{-2} cm s⁻¹.

As discussed in the previous section, at a depth insertion of about 6.0 Å, the pK_a and the pH equalize and, according to the Henderson–Hasselbach equation, $[Lys^+](z = 6.0) = [Lys^0](z = 6.0)$; i.e., the populations of neutral species and protonated species are identical. We consider therefore the lowest free-energy landscape encountered by a lysine during its passage through the membrane by building a hybrid free-energy profile combining the results obtained for the charged and the neutral species. As a crude approximation, this model free-energy profile can be obtained by merging part of the PMF associated with the transfer of the neutral lysine below $z = 6.0$ Å to the portion of the PMF associated with the charged lysine above $z = 6.0$ Å (Figure 5). Providing that the protonation switching

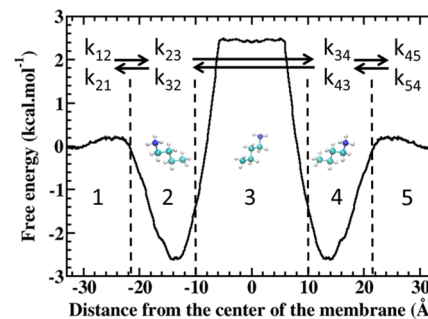


Figure 5. Merged free-energy profiles and rate constants associated with the transitions between the bulk media and the headgroup region, the headgroup region to the lipid core, the core to the other bilayer leaflet headgroup region, and then toward the opposite bulk media.

may occur on a wide range of distances, this model construct provides nevertheless a rough estimate of the time needed for a charged lysine to cross the membrane thanks to a deprotonation mechanism occurring at a given depth.

The translocation pathway was divided into different regions, bulk (1 and 5), headgroups (2 and 4), and the hydrophobic core (3). Accordingly, the rate constants associated with the lysine translocation between adjacent regions were determined using eqs 13 and 14: $k_{12} \approx 2.33 \times 10^9 \text{ s}^{-1}$, $k_{23} \approx 5.41 \times 10^5 \text{ s}^{-1}$, $k_{34} \approx 2.74 \times 10^9 \text{ s}^{-1}$, and $k_{45} \approx 2.75 \times 10^7 \text{ s}^{-1}$. Hence, the limiting process corresponds to the deprotonation step where the lysine goes from the headgroup to the hydrophobic core of the membrane.

Furthermore, the mean-passage time⁷⁴ associated with the transfer of the lysine analogue from the extracellular media to the cytoplasm was evaluated according to the protonation/deprotonation scheme

$$\tau = \int_a^b dz (e^{\beta \Delta G(z)} / D(z)) \int_{-\infty}^z dz' (e^{-\beta \Delta G(z')}) \quad (15)$$

where a and b are the positions on both side of the bilayer and z is the reaction coordinate. Interestingly, the value estimated here is $\sim 246 \mu\text{s}$, in agreement with the mean-passage time ($\sim 300 \mu\text{s}$) predicted for the transfer of the valproic acid across a dipalmitoyl-phosphatidyl-choline (DPPC) lipid bilayer.⁷⁵

The permeation coefficient inferred from the hybrid profile is $\sim 2.6 \times 10^{-1} \text{ cm s}^{-1}$, which is lower than that computed from the transfer of the neutral form only. This is consistent with the fact that compared to the merged profile, there is no significant barrier in the PMF associated with the transfer of the neutral lysine. Altogether, these results indicate that the permeation process of a lysine analogue through a POPC lipid bilayer occurs on the submilliseconds time scale, the limiting rate being the change of the protonation state in the headgroup region allowing the lysine to enter the hydrophobic core.

Influence of the Membrane Topology and Electrostatics—Ether to Ester Lipid Headgroups. In the following, we characterize the variation in the permeability of the lysine analogue in response to modifications of the lipid bilayer chemical pattern. For this purpose, bilayers formed by DPhPC lipids with either ester or ether linkage of the hydrocarbon chains to the glycerol backbone region were considered. Several structural differences between the two membranes have been reported,³⁰ among which was a lower area per lipid in the case of ether-DPhPC ($\sim 73 \text{ \AA}^2$) compared to ester-DPhPC ($\sim 79 \text{ \AA}^2$).³¹ The main difference however concerns the membrane dipole potential, which is twice lower for the ether lipid bilayer.²⁹

The PMFs associated with the transfer of the neutral form of the lysine analogue across both ester and ether-DPhPC bilayers derived using ABF are shown in Figure 6. The free-energy barriers at the entrance of the bilayer are on the same order of magnitude ($\sim 0.5 \text{ kcal mol}^{-1}$) as for POPC, which is consistent with the fact that the three lipid headgroups are chemically equivalent. In the ether lipid, this barrier appears around 24 \AA from the bilayer center, while it is located at 22 \AA for the ester lipid. The free-energy wells are also slightly shifted due to the different thickness of the two membranes, larger for ester than ether linkages (phosphates to phosphate distance in the bilayer: $d_{\text{ester}} = 36.84 \pm 0.56 \text{ \AA}$ vs $d_{\text{ether}} = 38.89 \pm 0.69 \text{ \AA}$). In the case of the ether membrane, the free-energy well is centered at $\sim 13.7 \text{ \AA}$ and is $-2.8 \text{ kcal mol}^{-1}$ deep compared to the bulk, while for the ester membrane the well is centered at $\sim 13 \text{ \AA}$ with a well of

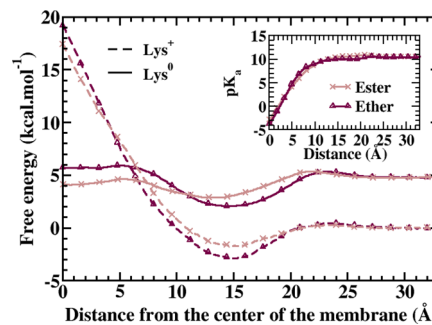


Figure 6. Free-energy transfer for both the neutral lysine (solid curve) and the charged lysine (dashed curve) in ether-DPhPC (maroon and triangles) and ester-DPhPC (brown and crosses) in 0.15 M [NaCl]. The neutral profile was shifted by the free-energy difference associated with the deprotonation reaction in the bulk. Inset: pK_a as a function of the depth for the lysine analogue in DPhPC with ester linkage (brown curve and crosses) and DPhPC with ether linkage (maroon curve and triangles). The lysine seems to remain charged deeper inside the membrane in the case of DPhPC with ether linkage than DPhPC with ester linkage.

$-2.5 \text{ kcal mol}^{-1}$ with respect to the bulk. Furthermore, the well is larger for the ether than for the ester membrane. Around the center of the bilayer, the free-energy difference with respect to the bulk is negative in the case of the ester membrane ($-1.2 \text{ kcal mol}^{-1}$) while it is positive ($0.8 \text{ kcal mol}^{-1}$) in the case of the ether membrane. Considering only the difference in the dipole potential (SM.4) of the ether and ester linkage bilayers can hardly explain this deviation between the two profiles at the core of the membranes. The density profiles of the ester and ether DPhPC bilayer are very similar (SM.1) and therefore do not provide strong evidence of variability that can be directly correlated with the changes in the free-energy profiles. We have estimated the local pressure profiles⁷⁶ along z , the bilayer normal. The pressure profiles were estimated from simulations as

$$p(z) = \frac{1}{\Delta V} \left[\sum_i m_i \mathbf{v}_i \otimes \mathbf{v}_i - \sum_{i < j} \mathbf{F}_{ij} \otimes \mathbf{r}_{ij} f(z, z_i, z_j) \right] \quad (16)$$

where $p(z)$ is the local pressure tensor in the slab centered on the coordinate z , the sum over the kinetic term running over all atoms in the slab and $f(z, z_i, z_j)$ a weighting function. The calculations were all performed on the fly⁴⁵ from the simulations performed at constant temperature and constant pressure. In lipid bilayers, the pressure profile variations are due to the amphiphatic nature of the lipids composing it: the hydrophilic head groups are squeezed together to prevent exposure of the hydrophobic tails to the solvent, leading to a negative lateral pressure, while the attractive dispersion forces and entropic repulsion between the lipid tails results mainly in a positive lateral pressure.

The comparison of the pressure profiles of ester- and ether-DPhPC (SM.6) shows a clear increase of (positive) lateral pressure in the middle for the ether bilayer. It is likely that such an increase in the local membrane lateral tension is at the origin of the increase of free energy of transfer of the lysine analogue.

For the charged lysine form, the free-energy profiles obtained in the bilayers are mainly similar. The free-energy well with respect to the bulk is slightly deeper in the ether membrane compared to that of the ester membrane ($-2.8 \text{ kcal mol}^{-1}$ and $-1.6 \text{ kcal mol}^{-1}$ respectively). Comparison of the pK_a profiles

between ester and ether lipid indicates that deprotonation occurs earlier (further from the bilayer center) in ester-DPhPC than in ether-DPhPC bilayers. Accordingly, the protonated lysine can be buried deeper in ether-DPhPC than in its ester counterpart or in a POPC (ester) membrane. The change in the lysine protonation state takes place at around 5.8 Å from the membrane center in ether, whereas it occurs at ~7.8 Å for the ester-lipid bilayer. This is mainly due to the fact that the ester-DPhPC membrane is ~2 Å thicker than the ether-DPhPC membrane; i.e., the headgroup region is shifted with respect to the center of the bilayer. Furthermore, it appears somewhat more difficult to bring a lysine (either in its neutral or charged form) at the center of an ether-DPhPC bilayer than an ester-DPhPC bilayer. The free-energy profiles associated with the transfer of a small hydrophobic nonpolar molecule, dioxygen, are similar irrespective of the presence of either ether or ester linkages.³⁰ In sharp contrast, it appears easier to transfer a polar molecule like water in the ester-linkage membrane compared to its ether counterpart.³⁰ The authors of the later study concluded that this difference is mainly rooted in the variation of the electrostatic potential at the center of the bilayer. These observations agree with our findings. Nevertheless, we demonstrated that a non-negligible contribution to the higher free-energy barrier, encountered by the lysine analogue in the case of the ester compared to the ether linkage, is also linked to the topology of the membrane.

The permeability and the mean-passage time associated with the transfer of the peptide across the ester membrane were estimated for ester and ether membranes, respectively, $P_{\text{ester}} = 2.1 \times 10^{-3} \text{ cm s}^{-1}$, $\tau_{\text{ester}} = 546 \mu\text{s}$ and $P_{\text{ether}} = 2.3 \times 10^{-4} \text{ cm s}^{-1}$, $\tau_{\text{ether}} = 2.6 \times 10^5 \mu\text{s}$.

These values were obtained by considering a hybrid profile following the same approximations as in the previous section. The permeation and the mean-passage time are lower in the case of the ether compared to the ester membrane, confirming kinetic experimental evidence for water molecules crossing membranes made out of different ether lipid varieties.³⁵ This result is consistent with the free-energy profiles exhibiting a higher barrier in the case of the ether membrane. Overall, the uptake of a lysine analogue is more favorable in the ester membrane.

Influence of the Lipid Tails—DPhPC vs POPC. This section emphasizes the differences occurring when the lysine amino acid analogue is driven inside a membrane constituted by lipids that differ in their tail structures. The ABF free-energy profiles for the neutral form show minor differences between DPhPC and POPC (see Figure 7).

The profiles for the protonated form show much more interesting features: while the barrier height at the center of the POPC bilayer is ~13.5 kcal mol⁻¹ (starting from the well located at 12.7 Å), it is ~19.5 kcal mol⁻¹ at the center of DPhPC bilayer (starting from the well located at 16 Å). It can also be noted that the slopes of the barriers in both cases are the same. In fact, by shifting the profile for POPC by ~3 Å in the direction of the bulk, the two free-energy profiles match nearly perfectly.

This is rather unexpected since the hydrophobic region in the DPhPC bilayer is a bit thicker than POPC bilayer (carbonyl to carbonyl distance $d_{\text{POPC}} = 27.96 \pm 0.82 \text{ \AA}$, $d_{\text{ester}} = 26.94 \pm 0.50 \text{ \AA}$), and the water density is even larger in the headgroup region for DPhPC compares to POPC (SI.1). The difference in the free-energy profiles is mainly due to the fact that POPC can support more easily local deformations to accommodate the

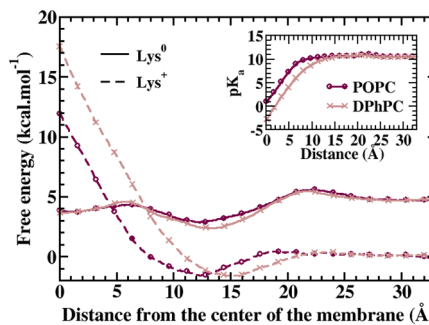


Figure 7. Free-energy transfer for both the neutral lysine (solid curves) and the charged lysine (dashed curves) in POPC (maroon and circles) and ester-DPhPC (brown and crosses) in 0.15 M [NaCl]. The neutral profile was shifted by the free-energy difference associated with the deprotonation reaction in the bulk. Inset: pK_a as a function of the depth for the lysine analogue in POPC (maroon curve and circles) and DPhPC with ester linkage (brown curve and crosses).

insertion of a charged compound compared to DPhPC, which is known to constitute more stable bilayers due to a higher entrapment, caused by the branched-carbon chains. This is in agreement with experimental observations on the stability of DPhPC-ester lipid based liposome where ion and proton leakage through the membrane was significantly lowered.^{36,77}

As a result, this has major influences on the pK_a profiles. The latter show that a charged compound cannot apparently be found deep inside a membrane constituted by branched lipids. Indeed, according to the pK_a profile, the position where $[\text{Lys}^+] = [\text{Lys}^0]$ is 8 Å from the center in DPhPC bilayer and 6 Å from the center of the bilayer in the case of POPC membranes.

The permeability and the mean-passage time associated with the transfer of the peptide across the DPhPC membrane was $P_{\text{DPhPC}} = 2.1 \times 10^{-3} \text{ cm s}^{-1}$, $\tau_{\text{DPhPC}} = 546 \mu\text{s}$ and $P_{\text{POPC}} = 2.5 \times 10^{-1} \text{ cm s}^{-1}$, $\tau_{\text{POPC}} = 240 \mu\text{s}$ for the POPC membrane. These values were obtained by considering a hybrid profile with the same approximations as in the last section. The uptake is lowered in the case of the ether-constituted membrane.

CONCLUSION

We investigated the mechanisms underlying the passive transfer of a small cationic compound (lysine amino acid analogue) through model membranes composed of POPC and DPhPC with either ether or ester linkage by means of molecular-dynamics simulations and free-energy calculations. Would such a compound permeate through the membrane, it would undergo a series of changes in its protonation state. pK_a calculations performed using two different computational approaches (alchemical transformation and ABF) showed that during the passage from the outermost bulk water to the bilayer hydrophobic core, the population of the lysine amino acid analogue in its neutral form becomes more and more important while the population of the charged form decreases. From a kinetic point of view, this transfer process appeared to be quite fast (submillisecond time scale); yet, it remains a rare event for the lysine analogue. Note that only one amino acid embedded in a patch of 64 lipid bilayer was considered here. Accordingly, our conclusions hold only for very low concentrations. At higher concentrations, other permeation characteristics may hold since this compound can act also as a surfactant modifying the properties of the lipid/water interface. Physico-chemical properties of the lipids modulate the thermodynamics and the kinetics features underlying the transfer process. Our data

emphasize that a decrease of the membrane dipole causes a decrease of the permeation coefficient of the polar compound, as shown previously.³⁰ Analysis of the pressure profile associated with the three bilayers considered in this work revealed that the rate transfer is not only modulated by electrostatics (affecting mainly the protonated form of the lysine analogue) but also depends on the fluidity of the membrane, the latter modifying the propensity of the neutral lysine to cross the bilayer. All together, our findings provide a precise picture of the transfer of titratable compounds often employed to enhance the capacity of drug nanovectors to cross membranes. We believe that the detailed knowledge of the protonation/deprotonation mechanism underlying the translocation process, and how the latter is modulated by the membrane composition, will help toward the rational design of effective nanovectors capable of conveying active substances in the cell.

ASSOCIATED CONTENT

Supporting Information

Density profiles, electrostatic potential profiles, and pressure profiles relative to the three types of membrane; diffusion profiles; and convergence of the PMFs. This material is available free of charge via the Internet at <http://pubs.acs.org>.

AUTHOR INFORMATION

Corresponding Authors

*E-mail: mounir.tarek@univ-lorraine.fr.

*E-mail: francois.dehez@univ-lorraine.fr.

Notes

The authors declare no competing financial interest.

ACKNOWLEDGMENTS

Calculations were performed at the Centre Informatique National de l'Enseignement Supérieur (Cines) Montpellier, France.

REFERENCES

- (1) Andreev, I.; Petrukhina, A.; Garmanova, A.; Babakhin, A.; Andreev, S.; Romanova, V.; Troshin, P.; Troshina, O.; DuBuske, L. *Fullerenes, Nanotubes, Carbon Nanostruct.* **2008**, *16*, 89–102.
- (2) Pantarotto, D.; Partidos, C. D.; Graff, R.; Hoebeke, J.; Briand, J.-P.; Prato, M.; Bianco, A. *J. Am. Chem. Soc.* **2003**, *125*, 6160–6164.
- (3) Isobe, H.; Nakanishi, W.; Tomita, N.; Jinno, S.; Okayama, H.; Nakamura, E. *Mol. Pharmaceutics* **2006**, *3*, 124–134.
- (4) Bianco, A.; Kostarelos, K.; Prato, M. *Chem. Commun.* **2011**, *47*, 10182–10188.
- (5) Hällbrink, M.; Florén, A.; Elmquist, A.; Pooga, M.; Bartfai, T.; Langel, Ü. *Biochim. Biophys. Acta, Biomembr.* **2001**, *1515*, 101–109.
- (6) Terrone, D.; Sang, S. L. W.; Roudaia, L.; Silvius, J. R. *Biochemistry* **2003**, *42*, 13787–13799.
- (7) Herce, H. D.; Garcia, A. E.; Litt, J.; Kane, R. S.; Martin, P.; Enrique, N.; Rebollo, A.; Milesi, V. *Biophys. J.* **2009**, *97*, 1917–1925.
- (8) Poland, C. A.; Duffin, R.; Kinloch, I.; Maynard, A.; Wallace, W. A.; Seaton, A.; Stone, V.; Brown, S.; MacNee, W.; Donaldson, K. *Nat. Nanotechnol.* **2008**, *3*, 423–428.
- (9) Vivès, E.; Schmidt, J.; Pèlegrin, A. *Biochim. Biophys. Acta, Rev. Cancer* **2008**, *1786*, 126–138.
- (10) Johnston, H. J.; Hutchison, G. R.; Christensen, F. M.; Aschberger, K.; Stone, V. *Toxicol. Sci.* **2010**, *114*, 162–182.
- (11) Eiríksdóttir, E.; Mäger, I.; Lehto, T.; El Andaloussi, S.; Langel, U. *Bioconjugate Chem.* **2010**, *21*, 1662–1672.
- (12) Gubernator, J. *Expert Opin. Drug Delivery* **2011**, *8*, 565–580.
- (13) Dorairaj, S.; Allen, T. W. *Proc. Natl. Acad. Sci. U. S. A.* **2007**, *104*, 4943–4948.
- (14) Johansson, A. C. V.; Lindahl, E. *Biophys. J.* **2006**, *91*, 4450–4463.
- (15) Li, L.; Vorobyov, I.; Allen, T. W. *J. Phys. Chem. B* **2008**, *112*, 9574–9587.
- (16) MacCallum, J. L.; Bennett, W. F. D.; Tielemans, D. P. *Biophys. J.* **2008**, *94*, 3393–3404.
- (17) Gleason, N. J.; Vostrikov, V. V.; Greathouse, D. V.; Koeppe, R. E. *Proc. Natl. Acad. Sci. U. S. A.* **2013**, *110*, 1692–1695.
- (18) Gumbart, J.; Roux, B. *Biophys. J.* **2012**, *102*, 795–801.
- (19) Åmand, H. L.; Fant, K.; Nordén, B.; Esbjörner, E. K. *Biochem. Biophys. Res. Commun.* **2008**, *371*, 621–625.
- (20) Singh, P.; Samorì, C.; Toma, F. M.; Bussy, C.; Nunes, A.; Al-Jamal, K. T.; Ménard-Moyon, C.; Prato, M.; Kostarelos, K.; Bianco, A. *J. Mater. Chem.* **2011**, *21*, 4850–4860.
- (21) Johansson, A. C. V.; Lindahl, E. *J. Chem. Phys.* **2009**, *130*, 185101–185108.
- (22) MacCallum, J. L.; Bennett, W. F. D.; Tielemans, D. P. *Biophys. J.* **2011**, *101*, 110–117.
- (23) Eriksson, E. S. E.; Eriksson, L. A. *J. Chem. Theory Comput.* **2011**, *7*, 560–574.
- (24) Yoo, J.; Cui, Q. *Biophys. J.* **2008**, *94*, L61–L63.
- (25) Starke-Peterkovic, T.; Clarke, R. J. *Eur. Biophys. J.* **2009**, *39*, 103–110.
- (26) Woese, C. R.; Kandler, O.; Wheelis, M. L. *Proc. Natl. Acad. Sci. U. S. A.* **1990**, *87*, 4576–4579.
- (27) Cavicchioli, R. *Nat. Rev. Microbiol.* **2010**, *9*, 51–61.
- (28) Husslein, T.; Newns, D. M.; Pattnaik, P. C.; Zhong, Q.; Moore, P. B.; Klein, M. L. *J. Chem. Phys.* **1998**, *109*, 2826–2832.
- (29) Wang, L.; Bose, P. S.; Sigworth, F. J. *Proc. Natl. Acad. Sci. U. S. A.* **2006**, *103*, 18528–18533.
- (30) Shinoda, K.; Shinoda, W.; Baba, T.; Mikami, M. *J. Chem. Phys.* **2004**, *121*, 9648–9654.
- (31) Polak, A.; Bonhenry, D.; Dehez, F.; Kramar, P.; Miklavčič, D.; Tarek, M. *J. Membr. Biol.* **2013**, *246*, 843–850.
- (32) Tenchov, B.; Vescio, E. M.; Sprott, G. D.; Zeidel, M. L.; Mathai, J. C. *J. Biol. Chem.* **2006**, *281*, 10016–10023.
- (33) Lai, D.; Springstead, J. R.; Monbouquette, H. G. *Extremophiles* **2007**, *12*, 271–278.
- (34) Shinoda, W.; Mikami, M.; Baba, T.; Hato, M. *J. Phys. Chem. B* **2003**, *107*, 14030–14035.
- (35) Dannenmuller, O.; Arakawa, K.; Eguchi, T.; Kakinuma, K.; Blanc, S.; Albrecht, A.-M.; Schmutz, M.; Nakatani, Y.; Ourisson, G. *Chem.—Eur. J.* **2000**, *6*, 645–654.
- (36) Haines, T. H. *Prog. Lipid Res.* **2001**, *40*, 299–324.
- (37) Yamauchi, K.; Doi, K.; Kinoshita, M. *Biochim. Biophys. Acta, Biomembr.* **1996**, *1283*, 163–169.
- (38) Humphrey, W.; Dalke, A.; Schulter, K. *J. Mol. Graphics* **1996**, *14*, 33–38.
- (39) Johansson, A. C. V.; Lindahl, E. *Proteins* **2008**, *70*, 1332–1344.
- (40) Johansson, A. C. V.; Lindahl, E. *J. Phys. Chem. B* **2009**, *113*, 245–253.
- (41) MacKerell, A. D., Jr.; Bashford, D.; Bellott, M.; Dunbrack, R. L.; Evanseck, J. D.; Field, M. J.; Fischer, S.; Gao, J.; Guo, H.; Ha, S.; Joseph-McCarthy, D.; Kuchnir, L.; Kuczera, K.; Lau, F. T. K.; Mattos, C.; Michnick, S.; Ngo, T.; Nguyen, D. T.; Prodhom, B.; Reiher, W. E.; Roux, B.; Schlenkrich, M.; Smith, J. C.; Stote, R.; Straub, J.; Watanabe, M.; Wiórkiewicz-Kuczera, J.; Yin, D.; Karplus, M. *J. Phys. Chem. B* **1998**, *102*, 3586–3616.
- (42) Klauda, J. B.; Venable, R. M.; Freites, J. A.; O'Connor, J. W.; Tobias, D. J.; Mondragon-Ramirez, C.; Vorobyov, I.; MacKerell, A. D., Jr.; Pastor, R. W. *J. Phys. Chem. B* **2010**, *114*, 7830–7843.
- (43) Feller, S. E.; Zhang, Y.; Pastor, R. W.; Brooks, B. R. *J. Chem. Phys.* **1995**, *103*, 4613–4621.
- (44) Martyna, G. J.; Tobias, D. J.; Klein, M. L. *J. Chem. Phys.* **1994**, *101*, 4177–4189.
- (45) Darden, T.; York, D.; Pedersen, L. *J. Chem. Phys.* **1993**, *98*, 10089–10092.
- (46) Essmann, U.; Perera, L.; Berkowitz, M. L.; Darden, T.; Lee, H.; Pedersen, L. G. *J. Chem. Phys.* **1995**, *103*, 8577–8593.

- (47) Izaguirre, J. A.; Reich, S.; Skeel, R. D. *J. Chem. Phys.* **1999**, *110*, 9853–9864.
- (48) Ryckaert, J.-P.; Ciccotti, G.; Berendsen, H. J. *J. Comput. Phys.* **1977**, *23*, 327–341.
- (49) Phillips, J. C.; Braun, R.; Wang, W.; Gumbart, J.; Tajkhorshid, E.; Villa, E.; Chipot, C.; Skeel, R. D.; Kalé, L.; Schulten, K. *J. Comput. Chem.* **2005**, *26*, 1781–1802.
- (50) Martínez, L.; Andrade, R.; Birgin, E. G.; Martínez, J. M. *J. Comput. Chem.* **2009**, *30*, 2157–2164.
- (51) Warshel, A.; Sussman, F.; King, G. *Biochemistry* **1986**, *25*, 8368–8372.
- (52) Veazey, W. R.; Hodgman, C. D. *Handbook of Chemistry and Physics*; Chemical Rubber Publishing Company: Boca Raton, FL, 1919; Vol. 8, p 47.
- (53) Zwanzig, R. W. *J. Chem. Phys.* **1954**, *22*, 1420–1426.
- (54) Pohorille, A.; Jarzynski, C.; Chipot, C. *J. Phys. Chem. B* **2010**, *114*, 10235–10253.
- (55) Darve, E.; Pohorille, A. *J. Chem. Phys.* **2001**, *115*, 9169–9183.
- (56) Hénin, J.; Chipot, C. *J. Chem. Phys.* **2004**, *121*, 2904–2914.
- (57) Darve, E.; Rodríguez-Gómez, D.; Pohorille, A. *J. Chem. Phys.* **2008**, *128*, 144120–144133.
- (58) Hénin, J.; Fiorin, G.; Chipot, C.; Klein, M. L. *J. Chem. Theory Comput.* **2010**, *6*, 35–47.
- (59) Boresch, S.; Karplus, M. *J. Phys. Chem. A* **1999**, *103*, 103–118.
- (60) Darve, E.; Pohorille, A. *J. Chem. Phys.* **2001**, *115*, 9169–9183.
- (61) Neale, C.; Bennett, W. F. D.; Tielemans, D. P.; Pomès, R. *J. Chem. Theory Comput.* **2011**, *7*, 4175–4188.
- (62) Orsi, M.; Essex, J. W. *Soft Matter* **2010**, *6*, 3797–3808.
- (63) Saito, H.; Shinoda, W. *J. Phys. Chem. B* **2011**, *115*, 15241–15250.
- (64) Wei, C.; Pohorille, A. *J. Phys. Chem. B* **2011**, *115*, 3681–3688.
- (65) Hummer, G. *New J. Phys.* **2005**, *7*, 34–48.
- (66) Wang, H.; Peskin, C. S.; Elston, T. C. *J. Theor. Biol.* **2003**, *221*, 491–511.
- (67) Liu, P.; Dehez, F.; Cai, W.; Chipot, C. *J. Chem. Theory Comput.* **2012**, *8*, 2606–2616.
- (68) Wilson, M. A.; Pohorille, A. *J. Am. Chem. Soc.* **1996**, *118*, 6580–6587.
- (69) Li, L.; Vorobyov, I.; Allen, T. W. *J. Phys. Chem. B* **2013**, *117*, 11906–11920.
- (70) Chakrabarti, A. C.; Deamer, D. W. *Biochim. Biophys. Acta, Biomembr.* **1992**, *1111*, 171–177.
- (71) Chakrabarti, A. C. *Amino Acids* **1994**, *6*, 213–229.
- (72) Walter, A.; Gutknecht, J. *J. Membr. Biol.* **1986**, *90*, 207–217.
- (73) Orsi, M.; Sanderson, W. E.; Essex, J. W. *J. Phys. Chem. B* **2009**, *113*, 12019–12029.
- (74) Szabo, A.; Schulten, K.; Schulten, Z. *J. Chem. Phys.* **1980**, *72*, 4350–4358.
- (75) Ulander, J.; Haymet, A. D. *J. Biophys. J.* **2003**, *85*, 3475–3484.
- (76) Lindahl, E.; Edholm, O. *Biophys. J.* **2000**, *79*, 426–433.
- (77) Yamauchi, K.; Doi, K.; Yoshida, Y.; Kinoshita, M. *Biochim. Biophys. Acta, Biomembr.* **1993**, *1146*, 178–182.